Article

Not peer-reviewed version

Total Hip Arthroplasty in Hip Osteoarthritis with Subtrochanteric Localized Periosteal Thickening: Preoperative Planning Using Finite Element Analysis to Determine the Optimal Stem Length

Koshiro Shimasaki , Tomofumi Nishino * , Tomohiro Yoshizawa , Ryunosuke Watanabe , Fumi Hirose , Shota Yasunaga , Hajime Mishima

Posted Date: 10 September 2024

doi: 10.20944/preprints202409.0767.v1

Keywords: atypical femoral fracture; finite element analysis; localized periosteal thickening; osteoarthritis; total hip arthroplasty

Case Report

Total hip Arthroplasty in Hip Osteoarthritis with Subtrochanteric Localized Periosteal Thickening: Preoperative Planning Using Finite Element Analysis to Determine the Optimal Stem Length

Koshiro Shimasaki, Tomofumi Nishino *, Tomohiro Yoshizawa, Ryunosuke Watanabe, Fumi Hirose, Shota Yasunaga and Hajime Mishima

Department of Orthopaedic Surgery, Institute of Medicine, University of Tsukuba, 1-1-1, Tennodai, Tsukuba, Ibaraki, 305-8575, Japan

* Correspondence: nishino@tsukuba-seikei.jp; Tel.: 029-853-7668

Abstract: Owing to the risk of atypical femoral fractures, total hip arthroplasty presents unique challenges for patients with ipsilateral osteoarthritis and localized periosteal thickening in the femoral subtrochanteric region. Stem length selection is critical for minimizing stress concentration in the thickened cortex to avoid such fractures. Herein, we report the case of a 78-year-old woman with ipsilateral hip osteoarthritis and localized subtrochanteric periosteal thickening. Preoperative planning included finite element analysis to assess stress distribution across various stem lengths. Simulation aimed to determine the optimal stem length to span the cortical thickening and reduce the risk of postoperative complications. The results of finite element analysis indicated that a stem length of >150 mm was required to effectively reduce the stress at the site of cortical thickening. A 175-mm stem was selected for total hip arthroplasty, which provided a favorable stress distribution and avoided the risk of stress concentration. Therefore, in cases of ipsilateral osteoarthritis with localized subtrochanteric periosteal thickening, finite element analysis can be valuable for preoperative planning to determine the optimal stem length, thereby reducing the risk of atypical femoral fractures. Further studies with multiple cases are recommended to validate these findings and improve surgical outcomes.

Keywords: atypical femoral fracture; finite element analysis; localized periosteal thickening; osteoarthritis; total hip arthroplasty

1. Introduction

The 2013 revision of the American Society for Bone and Mineral Research Task Force defines localized periosteal thickening of the femoral lateral cortex as a primary diagnostic criterion for atypical femoral fractures (AFFs) [1]. To avoid stress concentration, surgical interventions for an AFF generally involve using the longest possible intramedullary nails. While prophylactic intramedullary nailing is sometimes performed for localized cortical thickening, consensus regarding the appropriate surgical indications or timing is lacking. Moreover, careful monitoring is required as an AFF can develop with even minor trauma or a low-energy impact.

Total hip arthroplasty (THA) in the presence of ipsilateral osteoarthritis with localized cortical thickening is rare, with few reported cases. In a similar case report to ours, a stem of insufficient length was used, leading to the development of AFF postoperatively [2]. Although the stem tip might be positioned near the area of cortical thickening, potentially increasing the risk of an AFF due to concentrated stress, no studies have specifically addressed stem selection from the perspective of stress distribution.

Herein, we describe our experience in performing THA in a patient with ipsilateral osteoarthritis of the hip and localized cortical thickening in the subtrochanteric region of the femur. The procedure

 doi:10.20944/preprints202409.0767.v1

planning was guided by preoperative finite element method (FEM) simulation to assess femoral stress distribution.

In this study, we focused on stem length and conducted three-dimensional (3D) simulations using FEM to evaluate stress distributions in stems of varying lengths, ultimately guiding our stem selection. Moreover, we considered and emphasized treatment strategies for ipsilateral osteoarthritis with localized cortical thickening. We hypothesized that the longer the bridging length of the stem over the thickened cortex, the greater the stress reduction in that area. To the best of our knowledge, this study is the first to examine the relationship between stem length and stress distribution in local femoral cortical thickening using FEM.

2. Case Description

2.1. Case Presentation

A 78-year-old woman without a history of developmental hip dysplasia had been diagnosed with systemic lupus erythematosus at 46 years of age. The initial treatment involved steroid pulse therapy, followed by continuous oral prednisolone thereafter. Concurrently, treatment with 200 mg etidronate was initiated for glucocorticoid-induced osteoporosis. After 47 days, the medication was switched from etidronate to 35 mg alendronate, which was continued thereafter.

At 73 years of age, the patient experienced a fall and was diagnosed with a left subtrochanteric AFF based on plain radiography and computed tomography (CT) findings. Additionally, localized lateral cortical thickening was observed in the ipsilateral subtroschanteric region, along with osteoarthritis of the right hip (Figure 1). The patient underwent open reduction and internal fixation with an intramedullary nail for the left subtrochanteric AFF. Alendronate was discontinued, and treatment comprising 600 μg teriparatide (recombinant) was initiated, which was continued for 2 years. Due to nonunion at the fracture site, the patient underwent surgery for pseudarthrosis at 75 years of age (Figure 2). Given the gradual worsening of the right hip osteoarthritis, THA was planned when the patient turned 78 years of age.

 doi:10.20944/preprints202409.0767.v1

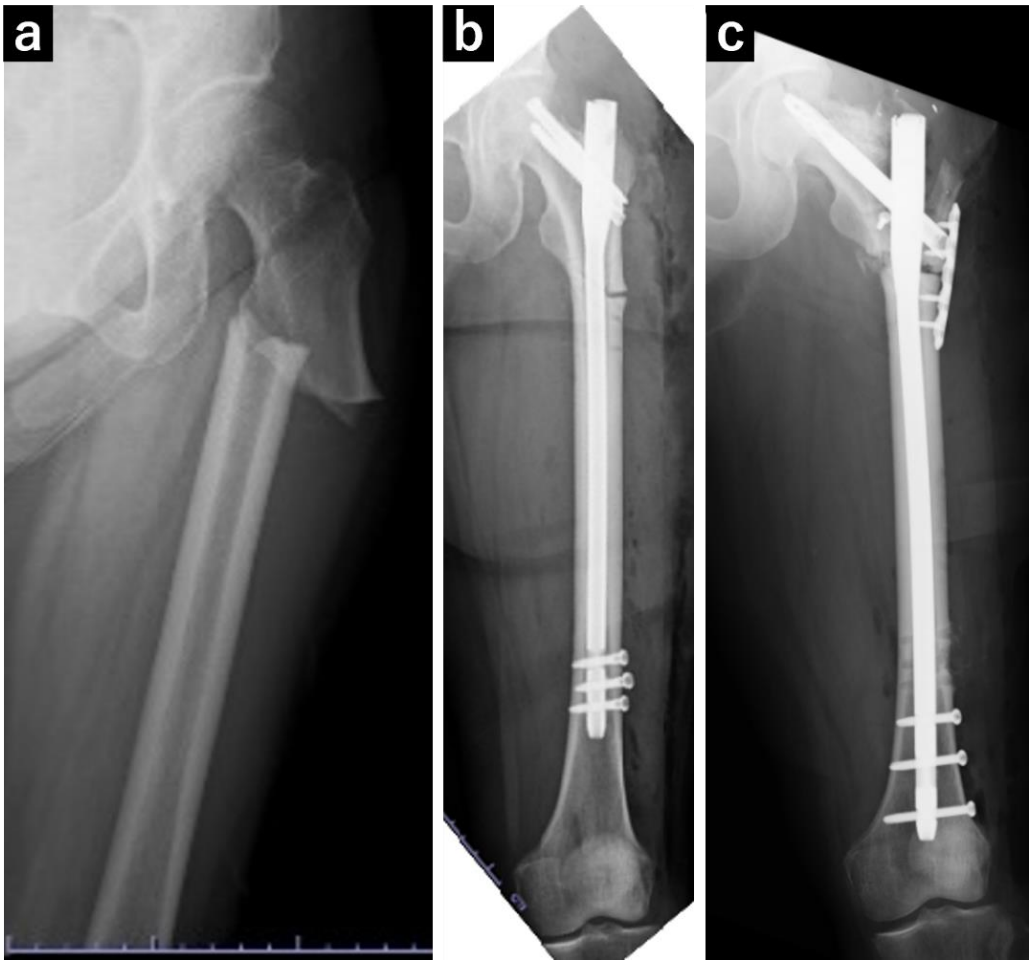

Figure 1. Plain radiograph of the left femur. (**a**) A transversal fracture in the subtrochanteric region of the left femur diagnosed as an atypical femoral fracture. (**b**) Postoperative image following open reduction and internal fixation of the atypical femoral fracture. (**c**) Postoperative image following surgery for pseudarthrosis of the left femur, in which replacement with a long nail and additional plate fixation were performed.

 doi:10.20944/preprints202409.0767.v1

Figure 2. Plain radiograph and computed tomography (CT) images of the right femur. (**a**) Plain radiograph showing localized cortical hypertrophy at the subtrochanteric region. (**b**) Plain CT image showing no obvious radiolucent lines. (**c**) A full-length plain radiograph of the lower limbs showing no significant femoral bowing deformity.

2.2. Finite Element Analysis

Informed consent was obtained from the patient for using and publishing these data, and this retrospective study was approved by the ethics review committee of our institution (approval code: H27-041).

We performed preoperative 3D simulations using FEM to analyze stress distributions in the femur following stem insertion. We also evaluated the stress distributions at the site of cortical thickening for different stem lengths.

3. Methods

3.1. Three-Dimensional Modeling of the Femur and Implant

Preoperative CT was performed using a 256-slice multidetector CT scanner (Brilliance iCT; Philips Healthcare, Cleveland, Ohio, USA). The scan, which included a bone mineral density phantom (QRM-BDC/3 Phantom, QRM Quality Assurance in Radiology and Medicine GmbH, Möhrendorf, Germany), captured images from the pelvis to both knee joints (120 kV/166 mAs, 1-mm thin slice).

First, based on CT images, we simulated stem insertion using the ZedHip 3D preoperative planning software (Lexi Co., Ltd, Tokyo, Japan). The patient in this case had a narrow medullary canal and mild anterior bowing of the femoral shaft. As the selection of stems that could span the area of cortical hypertrophy and fit the femoral morphology of the patient was limited, we opted for

 doi:10.20944/preprints202409.0767.v1

the Arcos® One-piece Femoral Revision System (Zimmer, Warsaw, Indiana, USA) with a 9.5 mm diameter and 175 mm length, in the high offset configuration.

We then generated Standard Triangulated Language (STL) data for stems of varying lengths. The original stem STL data were imported into the 3D computer-aided design software Fusion 360 (Autodesk, San Francisco, CA, USA) and modified using the "cut" and "join" functions. The stem lengths included the original size of 175 mm, a 115-mm stem aligned with the level of cortical thickening at the stem tip, and additional lengths ranging from 90 mm to 180 mm in 10-mm increments (Figure 3). The 90-mm stem was the shortest length that could be generated without altering the proximal stem geometry, while 180-mm was the maximum length that could be inserted with the same alignment.

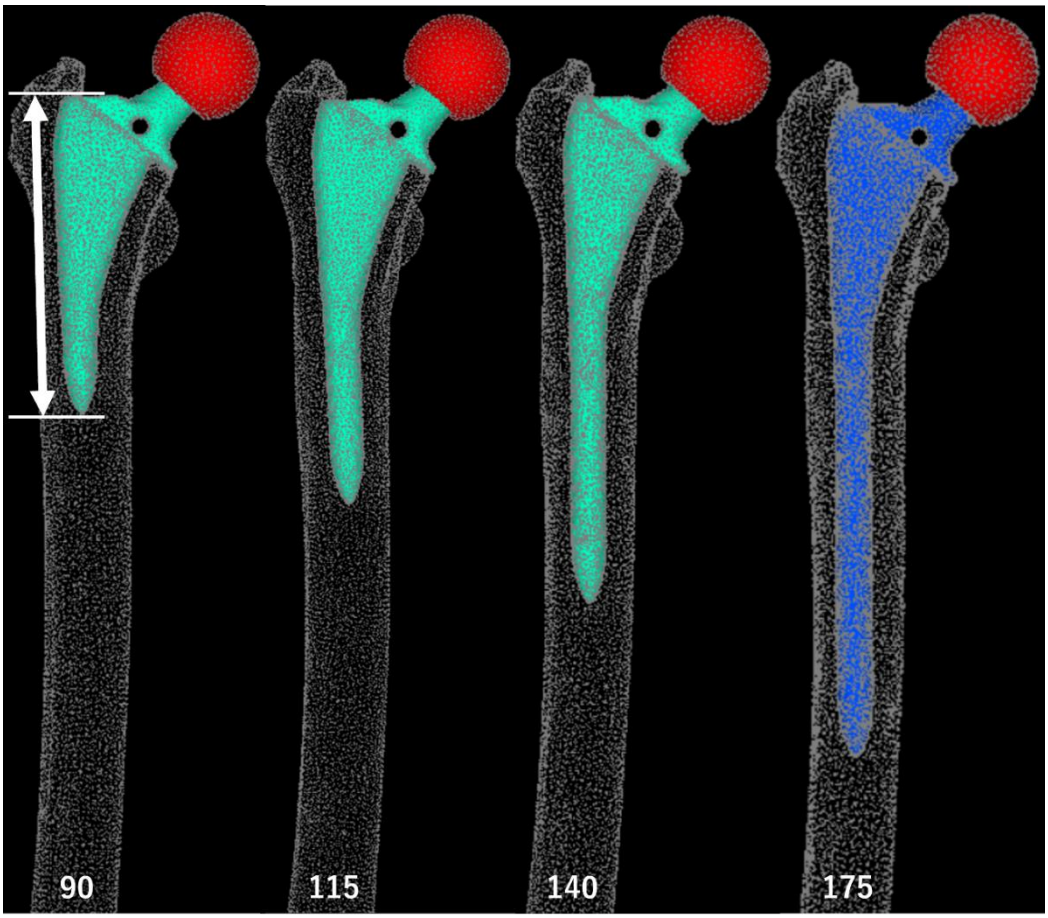

Figure 3. Standard Triangulated Language data for stems of varying lengths. White arrows: stem lengths. The 90-mm stem length corresponds to a position 25 mm proximal to the thickened region (equivalent to 1 femoral cortical diameter), the 115-mm stem length corresponds to the level of the thickened cortical region, and the 140-mm stem length corresponds to 25-mm (1 femoral cortical diameter) bridging length over the thickened area. A 175-mm stem was used in the actual surgery.

Next, we constructed a 3D model of the right femur. Preoperative CT data were imported into the FEM analysis software MECHANICAL FINDER (MF, version 13.0, Extended Edition, Research Center of Computational Mechanics, Tokyo, Japan), where bone was defined as an area with a density of ≥300 Hounsfield Units (HU). Only the right femur was extracted. We generated a model of the femur by performing an osteotomy at the proximal level 10 mm above the lesser trochanter and creating an isosurface mesh to represent the external shape of the femur.

By registering the acquired stem STL data with a 3D model of the right femur in MF, we were able to replicate femur post-stem insertion. The insertion depth and alignment of the stem were reproduced in MF based on the simulation conducted in ZedHip, ensuring consistency in 3D coordinates across the analysis of each stem (Figure 4).

 doi:10.20944/preprints202409.0767.v1

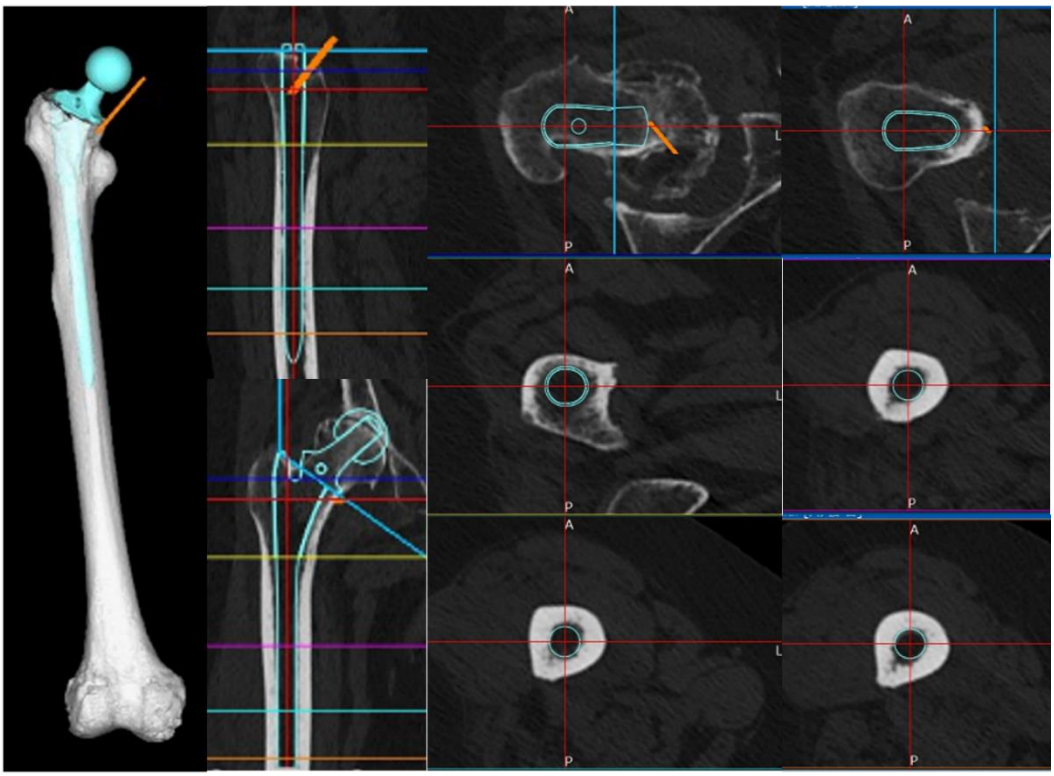

Figure 4. Stem insertion depth and alignment. Preoperative planning was performed using three-dimensional (3D) ZedHip software. The stem was planned to be inserted at a 32° anteversion angle relative to the condylar axis on the femoral horizontal section, a 3° valgus angle relative to the femoral axis on the femoral coronal section, a 5° flexion angle relative to the femoral axis on the femoral sagittal section, and a depth of 11 mm from the apex of the greater trochanter.

3.2. Material Properties

We used four-node tetrahedron elements for the solid components. For stress analysis, shell elements with a thickness of 0.001 mm were applied to the bone surface to ensure that they did not affect bone strength.We conducted mesh convergence tests to determine the mesh size.

3.2.1. Bone Material (Femur)

We set the internal mesh size to minimum and maximum values of 1 mm and 2 mm, respectively, and employed a heterogeneous material model for the bone properties. The Young's modulus was derived using bone mineral density (BMD, ϱ (g/cm^3)), calculated from the CT values (HU) based on an assumed linear relationship [3,4]. Then, the values were estimated using Keyak's predictive transformation formula and incorporated into the model. Poisson's ratio was set to 0.40 [5].

3.2.2. Other Materials (Stem and Artificial Head)

For these components, we set the internal mesh size to a minimum of 0.5 mm and a maximum of 1 mm. This study used a model with homogeneous material. The stem was modeled using the material properties of a titanium alloy (Ti-6Al-4V) with a Young's modulus of 109 GPa and Poisson's ratio of 0.28. For the artificial head, we used a ceramic (alumina) with a Young's modulus of 350 GPa and Poisson's ratio of 0.23.

3.3. Loading and Boundary Conditions

We designed the loading conditions to simulate the forces encountered during daily activities. We applied the maximum loads corresponding to "normal walking" and "stair climbing" based on

 doi:10.20944/preprints202409.0767.v1

previous reports [6,7]. The "stair-climbing" scenario allowed for the examination of higher load forces and stronger torques than "normal walking." The magnitude of each vector was determined by the patient's body weight (50.4 kg), with the load acting as shown in Table 1 and Figure 5.

Table 1. Loading during simulated "normal walking" and "stair-climbing" scenarios.

Normal walking, Right	**B.W (N)=**	**504**				
Force	**X (N)**	**Y (N)**	**Z (N)**	**Loading point**	**(%)**	**Load (N)**
Hip contact	-54.0	32.8	-229.2	P0	238	1199.52
ABD	-58.0	4.3	86.5	P1	104	
TFL-P	-7.2	11.6	13.2	P1	19	
TFL-D	0.5	-0.7	-19.0	P1	19	
P1 total force	64.7	-15.2	80.7	P1	105	529.2
VL	0.9	-18.5	-92.9	P2	95	478.8

Stair climbing, Right	**B.W (N)=**	**504**				
Force	**X (N)**	**Y (N)**	**Z (N)**	**Loading point**	**(%)**	**Load (N)**
Hip contact	-59.3	60.6	-236.3	P0	251	1265.04
ABD	-70.1	28.8	84.9	P1		
ITT-P	-10.5	3.0	12.8	P1		
ITT-D	0.5	-0.8	-16.8	P1		
TFL-P	-3.1	4.9	2.9	P1		
TFL-D	0.2	-0.3	-6.5	P1		
P1 total force	83.0	-35.6	77.3	P1	119	599.76
VL	2.2	-22.4	-135.1	P2	137	690.48
VM	8.8	39.6	-267.1	P3	270	1360.8

ABD: abductor; TFL: tensor fascia latae; -P: proximal; -D: distal; VL: vastus lateralis; VM: vastus medialis.

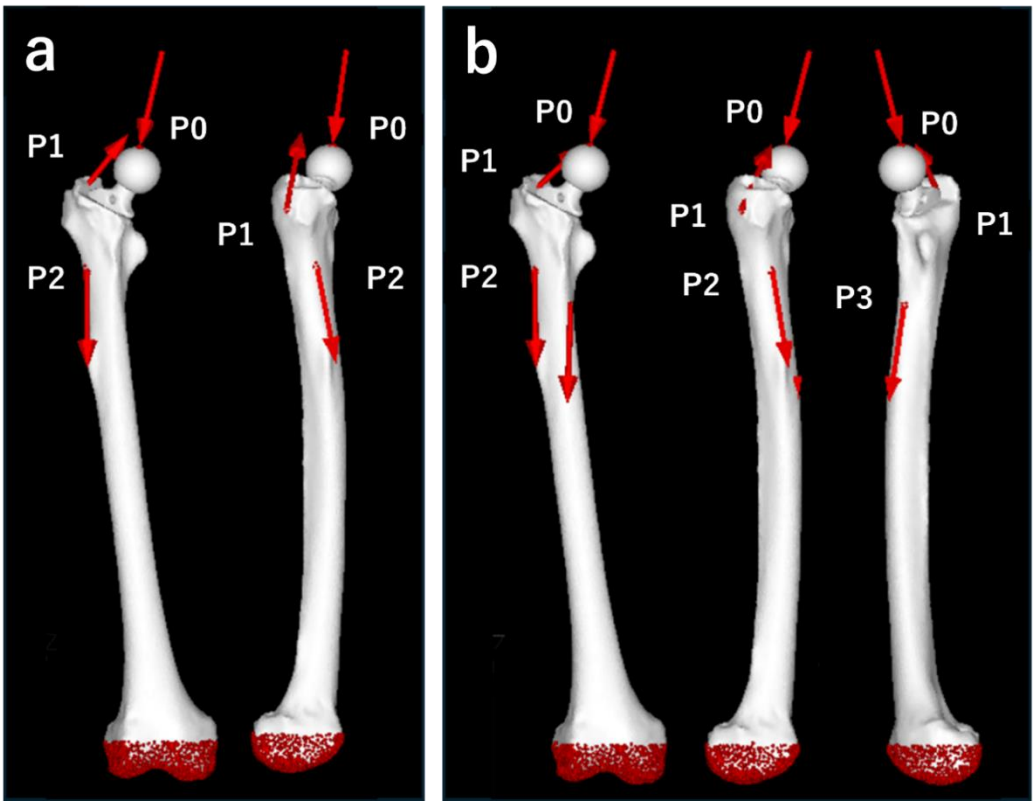

 doi:10.20944/preprints202409.0767.v1

Figure 5. Loading points and fixation sites for simulated normal walking and stair climbing. (**a**) Normal walking. P0: hip contact point; P1: the combined force of the abductor muscles and iliotibial band; P2: action point of the vastus lateralis. (**b**) Stair climbing. P0: hip contact point; P1: combined force of the abductor muscles, iliotibial band, and tensor fasciae latae; P2: action point of the vastus lateralis; P3: action point of the vastus medialis. In both conditions, the distal femur was fully constrained.

For the constraint conditions, the distal part of the femur was fixed (Figure 4). The boundary conditions included a fixed connection between the stem and head, and a contact condition with a friction coefficient of 0.49 between the femur and stem [8].

3.4. Static Structural Analysis

We conducted simulations under normal walking and stair-climbing conditions using stems of varying lengths. Elastic analysis was performed with the load gradually increasing linearly, and linear static analysis was applied to the calculations. We used equivalent stress (MPa) as the measure of stress and calculated the overall stress distributions across the femur, as well as the average and maximum equivalent stress values in the area of cortical thickening. The hypertrophic region was standardized to 40 mm in width and 60 mm in length along the bone axis, centered around the apex of the hypertrophic area to encompass the entire hypertrophic region. The calculations considered only the stress values of the femoral surface shell elements (Figure 6).

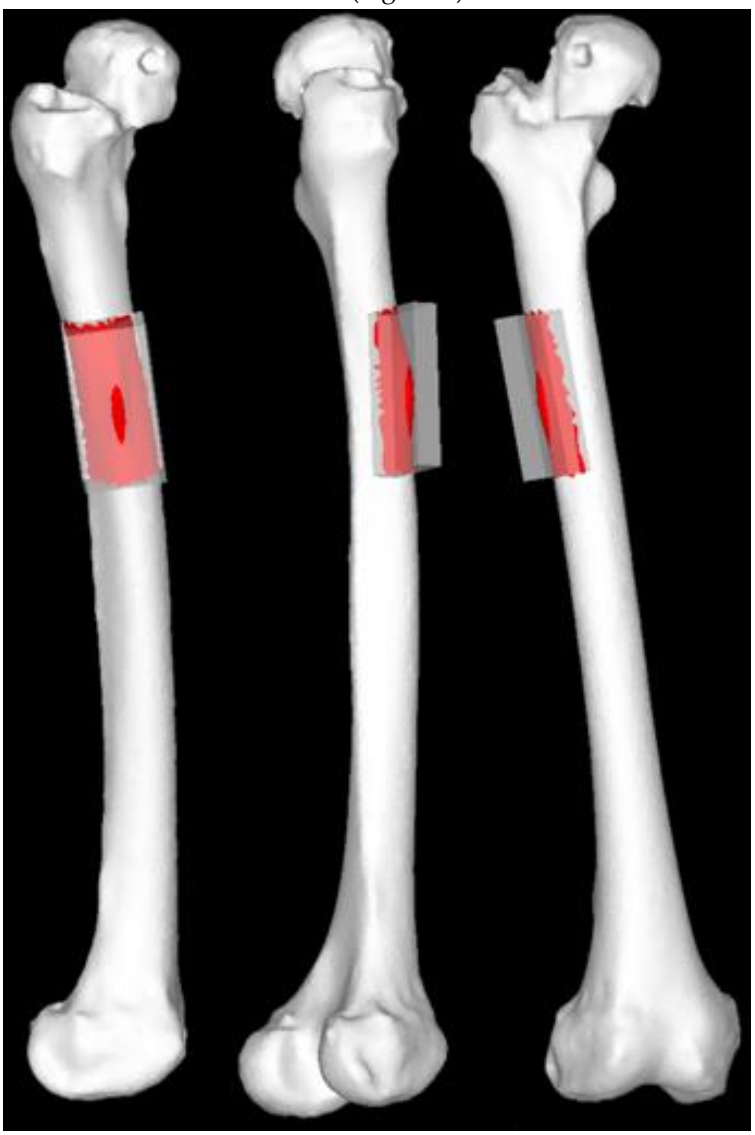

 doi:10.20944/preprints202409.0767.v1

Figure 6. Regions of interest for stress value calculations. The regions of interest included the femoral surface shell elements within a 40-mm wide and 60-mm axial-long area centered around the apex of the area of cortical hypertrophy to encompass the entire hypertrophic area.

4. Results

The number of elements comprising each model is shown in Table 2.

Figure 7 shows the stress distributions across the lateral surface of the femur for each model during normal walking and stair-climbing conditions. Figure 8 illustrates the mean and maximum equivalent stress values in the region of cortical thickening. The stress distribution across the lateral surface of the femur decreased following stem insertion. No new areas of stress concentration were observed during normal walking or stair-climbing conditions.

Table 2. The number of components for each model.

Stem length [mm]	Number of elements
Control	411,681
90	589,149
100	595,689
110	618,600
120	631,146
130	640,215
140	656,649
150	667,911
160	673,071
170	681,366
180	681,891

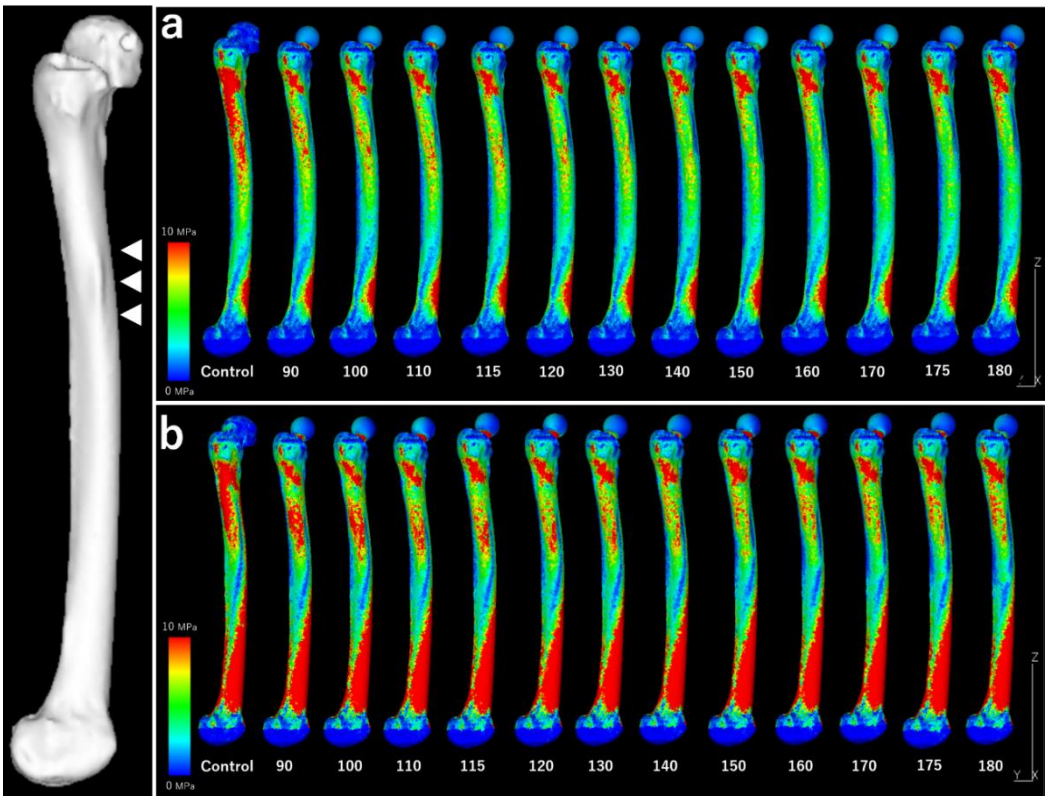

Figure 7. Stress distributions across the entire lateral femoral surface. White arrow: Localized periosteal thickening. (**a**) "Normal walking." (**b**) "Stair climbing." Under both conditions, the stress

 doi:10.20944/preprints202409.0767.v1

around the cortical hypertrophy area decreased as the stem length increased. No new stress concentrations are observed.

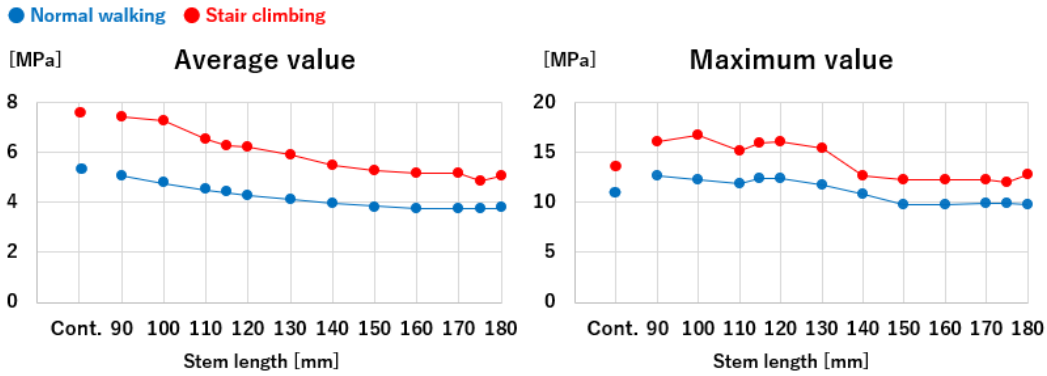

Figure 8. Stem lengths and equivalent stresses in the cortical hypertrophic areas. The equivalent stresses in the cortical hypertrophic areas followed trends closely approximated by curves as a function of stem length.

The mean equivalent stress at the thickened region decreased gradually as stem length increased, following an approximation curve. The stress nearly plateaued at a length of 120 mm during normal walking and 150 mm during stair climbing, with approximately the same level as the control. Similarly, the maximum stress decreased with increasing stem length, following a trend similar to the mean values. However, elevated stress levels were observed near a stem length of 115 mm, where the stem tip overlapped with the thickened region during normal walking and stair-climbing conditions. Beyond this length, where the stem tip extended past the thickened area, the stress followed a decreasing approximation curve. The stress values plateaued at a length of approximately 150 mm, which was almost identical to that of the control.

Based on the abovementioned findings, we performed THA using a posterior approach (Figure 9). Postoperatively, full weight bearing on the affected limb was allowed. The patient could walk with a cane and was transferred to another hospital for rehabilitation on postoperative day 14. At the final follow-up (3 months postoperatively), the patient could walk independently and experienced no difficulties in daily activities.

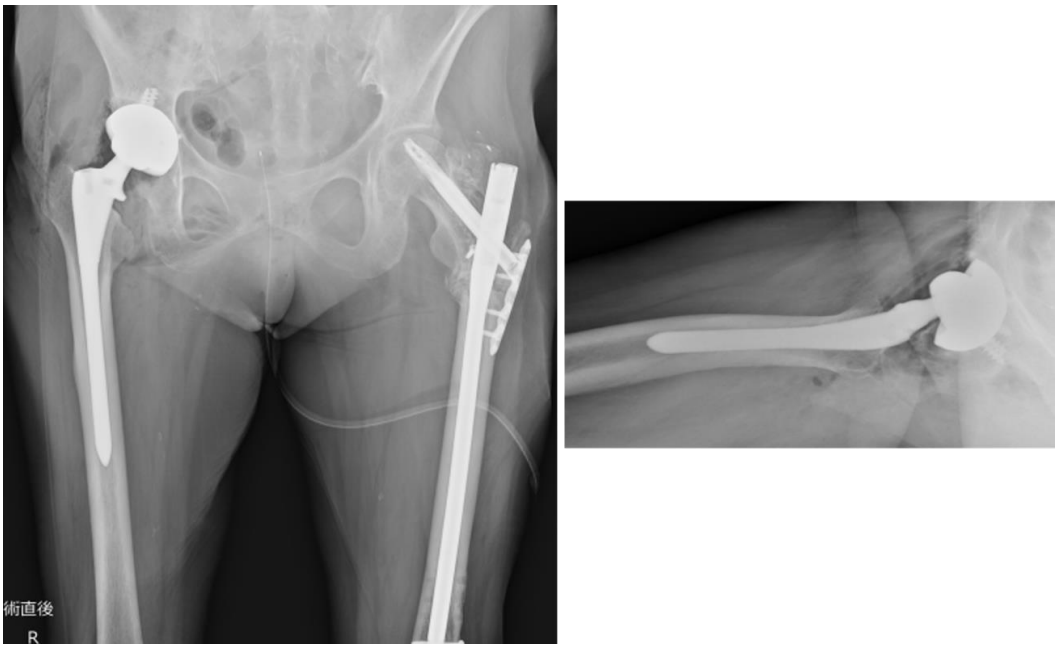

Figure 9. Plain radiograph of the hip joint immediately postoperatively. The stem (Arcos® One-piece Femoral Revision System, Zimmer, Warsaw, Indiana, USA, φ9.5 mm × 175 mm, high offset) was

 doi:10.20944/preprints202409.0767.v1

inserted to a depth of 11 mm below the apex of the greater trochanter, as planned preoperatively. The cup (Continuum®, Zimmer, Warsaw, Indiana, USA, Φ28/46 mm) was fixed and positioned using four screws. The surgery was completed in 1 h 20 min, with a blood loss of 50 ml.

4. Discussion

Preoperative 3D simulation conducted using FEM to evaluate stress distribution at the site of localized cortical thickening revealed reduced stress along the femur's lateral surface after stem insertion, without introducing new stress concentrations during normal walking or stair-climbing conditions. The stress at the cortical thickening progressively decreased and stabilized at approximately 120 mm for walking and 150 mm for stair climbing. The maximum stress initially peaked near the 115 mm stem length, where the stem tip corresponded with cortical thickening, but diminished and plateaued with longer stems, particularly beyond 150 mm.

AFFs tend to develop gaps on the medial side of the fracture because of the mismatch between femoral morphology and implants, making nonunion more likely [9–11]. Furthermore, long-term use of bone resorption inhibitors; over-suppression of bone turnover due to metabolic diseases; and decreased bone quality associated with collagen diseases, rheumatoid disorders, or glucocorticoid use can all contribute to delayed bone healing [9,12,13]. The subtrochanteric region is particularly challenging because it consists predominantly of cortical bone with a poor blood supply, making stable fixation of the fracture challenging. Additionally, adequate medial support is difficult to secure due to the transverse or oblique nature of AFFs. These anatomical complexities make bone healing difficult, rendering subtrochanteric AFFs particularly refractory [14]. Therefore, strict management of femoral cortical hypertrophy to prevent progression to an AFF is crucial not only for maintaining patients' activities of daily living and quality of life but also from a healthcare economic perspective.

Conservative treatment for femoral cortical hypertrophy primarily involves discontinuing bisphosphonate (BP) therapy and imposing weight-bearing restrictions on the affected limb [9]. The risk of AFF progression decreases rapidly following BP therapy cessation [15]. Additionally, PTH therapy may effectively promote bone healing in cases of AFFs [16]. Although surgical treatment with intramedullary nailing for femoral cortical hypertrophy has a high bone union rate of 95–98% [17], clear consensus is lacking regarding the indications for prophylactic surgery or the optimal timing for such interventions.

Min et al. proposed a scoring system to assess the risk of progression from localized cortical hypertrophy to an AFF, considering four factors: (1) location, (2) pain, (3) contralateral fracture presence and severity, and (4) radiolucent lines. Each factor was scored from 1 to 3 points, with a total score of ≥8 points indicating the need for prophylactic surgery [17].

Additionally, Joaquin et al. recommended evaluating femoral cortical hypertrophy using CT, magnetic resonance imaging, and bone scanning [2]. They categorized cortical hypertrophy into four stages based on the presence of lucent lines and marrow edema: "stress reaction," "stress fracture," "incomplete AFF," and "complete AFF" and proposed a flowchart for management and treatment strategies for each stage.

In the present case of localized cortical hypertrophy, the Min BW scoring system resulted in a total of 6 points (2 points for location, 2 points for pain, 1 point for contralateral fractures, and 1 point for radiolucent lines), which is below the threshold of 8 points for recommending prophylactic surgery. According to the flowchart proposed by Joaquin et al., the preoperative simple CT scan did not reveal lucent lines, suggesting that the condition could be classified as either "stress reaction" or "stress fracture."

Based on this assessment, we concluded that a surgical intervention was not warranted for localized cortical hypertrophy. However, given the risk of stress concentration in the hypertrophic area due to stem insertion, progression to a fracture during the postoperative period was possible. Therefore, we determined that using a sufficiently long stem to bridge the cortical hypertrophy and avoid postoperative stress concentration was essential.

THA in the presence of localized cortical hypertrophy and concomitant osteoarthritis of the same hip is rare, with few reported cases [2,18]. Yee et al. reported a case in a 72-year-old woman with a

 doi:10.20944/preprints202409.0767.v1

complete AFF in the subtrochanteric region associated with same-sided osteoarthritis, in which THA was performed using an uncemented stem and additional reinforcement with a plate and wiring [18]. Similarly, Joaquin et al. documented a 66-year-old woman in whom an incomplete AFF in the subtrochanteric region associated with osteoarthritis progressed to a complete AFF after THA, necessitating additional surgery with wiring fixation of the fracture site. The authors suggested bridging the fracture site with cemented or long revision stems combined with wire or lateral plate fixation [2]. However, these previous reports did not provide specific recommendations regarding the optimal stem length.

Strategies for managing Vancouver classification type B2 or B3 periprosthetic fractures around artificial hips may provide useful guidance for bridging the fracture site with a stem. The standard approach for type B2 or B3 fractures involves removing any existing stem loosened due to the fracture and replacing it with a sufficiently long stem that bridges the fracture site [19].

Several studies have proposed various options for stem selection. For example, all-porous-coated uncemented stems are recommended to bridge the fracture site with additional reinforcement using plates and wires or cemented stems to bridge the fracture site [1,19]. Regarding stem length, biomechanical studies using model bones suggest that the revision stem should bypass the fracture site by at least two cortical diameters to ensure adequate stabilization [20–22].

The FEM simulations conducted in this study with various stem lengths yielded results consistent with those of previous reports, suggesting the use of sufficiently long stems to bridge vulnerable areas. The maximum load during daily activities must include the maximum stress during stair climbing. The transverse diameter of the cortical hypertrophy in the present case was 25 mm, and the bridging length of the cortical hypertrophy with a 150 mm long stem corresponds to 1.4 femoral cortex diameters. This was 30% shorter than the two femoral cortex diameters recommended for fracture management in previous reports [20–22].

For localized cortical hypertrophy, as opposed to complete fractures, the axial stability of the implant bridging is less critical. Therefore, a shorter stem length should be adequate for bridging cortical hypertrophy, as indicated in this study. Given the limited variation in stem lengths available for clinical use, a stem >150 mm in bridging length that is physically insertable should be used. The 175 mm stem used in this case was deemed to be of sufficient length from the perspective of stress distribution.

This study used data from a single female patient. For simplicity, we focused solely on stem length, without analyzing other factors that could affect stress distribution, such as stem shape or diameter. Ideally, verification through experimental studies with simulated or cadaveric bones would be beneficial; however, creating reproducible models for such validation is challenging. Thus, we recommend further validation using FEM in multiple similar cases. Additionally, the postoperative observation period was limited to 3 months in the present case. Thus, as long-term stress distributions in cortical hypertrophy areas remain unknown, careful monitoring is necessary.

5. Conclusions

In the present case of femoral osteoarthritis with localized cortical hypertrophy in the subtrochanteric region, we performed FEM-based preoperative planning and used a long stem revision for THA. From the perspective of stress distribution, a stem length >150 mm (a bridging length of 1.4 femoral cortical diameters) is required to bridge the area of cortical hypertrophy. The 175 mm stem used in this case was sufficient for stress distribution.

Author Contributions: Conceptualization: K.S.; methodology: K.S.; software: K.S., R.W.; validation: K.S.; formal analysis: K.S.; investigation: K.S., F.H., and S.Y.; resources: K.S., F.H., S.Y., R.W., and T.Y.; writing—original draft preparation: K.S.; writing—review and editing: T.N., F.H., S.Y., R.W., T.Y., and H.M.; visualization: K.S.; supervision: T.N., R.W., T.Y., and H.M.; project administration: T.N., R.W., T.Y., and H.M. All authors have read and agreed to the published version of the manuscript.

Funding: This research received no external funding.

Institutional Review Board Statement: This retrospective study was approved by the Ethics Committee of the University of Tsukuba Hospital on August 14, 2022 (approval code: H27-041).

 doi:10.20944/preprints202409.0767.v1

Informed Consent Statement: Informed consent was obtained from all participants involved in the study.

Data Availability Statement: The data are available from the corresponding author upon reasonable request.

Acknowledgments: The authors would like to thank Editage (http://www.editage.jp/) for English language editing.

Conflicts of Interest: The authors declare no conflicts of interest.

References

1. Shane, E.; Burr, D.; Abrahamsen, B.; Adler, R.A.; Brown, T.D.; Cheung, A.M.; Cosman, F.; Curtis, J.R.; Dell, R.; Dempster, D.W.; Ebeling, P.R.; Einhorn, T.A.; Genant, H.K.; Geusens, P.; Klaushofer, K.; Lane, J.M.; McKiernan, F.; McKinney, R.; Ng, A.; Nieves, J.; O'Keefe, R.; Papapoulos, S.; Howe, T.S.; van der Meulen, M.C.; Weinstein, R.S.; Whyte, M.P. Atypical subtrochanteric and diaphyseal femoral fractures: second report of a task force of the American Society for Bone and Mineral Research. *J Bone Miner Res* **2014**, 29, 1–23, DOI:10.1002/jbmr.1998.
2. Moya-Angeler, J.; Zambrana, L.; Westrich, G.H.; Lane, J.M. Atypical femoral fracture post total hip replacement in a patient with hip osteoarthritis and an ipsilateral cortical thickening. *Hip Int* **2016**, 26, e19–23, DOI:10.5301/hipint.5000305.
3. Hirata, Y.; Inaba, Y.; Kobayashi, N.; Ike, H.; Fujimaki, H.; Saito, T. Comparison of mechanical stress and change in bone mineral density between two types of femoral implant using finite element analysis. *J Arthroplasty* **2013**, 28, 1731–1735, DOI:10.1016/j.arth.2013.04.034.
4. Tano, A.; Oh, Y.; Fukushima, K.; Kurosa, Y.; Wakabayashi, Y.; Fujita, K.; Yoshii, T.; Okawa, A. Potential bone fragility of mid-shaft atypical femoral fracture: Biomechanical analysis by a CT-based nonlinear finite element method. *Injury* **2019**, 50, 1876–1882, DOI:10.1016/j.injury.2019.09.004.
5. Keyak, J.H.; Rossi, S.A.; Jones, K.A.; Skinner, H.B. Prediction of femoral fracture load using automated finite element modeling. *J Biomech* **1998**, 31, 125–133, DOI:10.1016/s0021-9290(97)00123-1.
6. Bergmann, G.; Bender, A.; Dymke, J.; Duda, G.; Damm, P. Standardized loads acting in hip implants. *PLoS One* **2016**, 11, e0155612, DOI:10.1371/journal.pone.0155612.
7. Heller, M.O.; Bergmann, G.; Kassi, J.P.; Claes, L.; Haas, N.P.; Duda, G.N. Determination of muscle loading at the hip joint for use in pre-clinical testing. *J Biomech* **2005**, 38, 1155–1163, DOI:10.1016/j.jbiomech.2004.05.022.
8. Biemond, J.E.; Aquarius, R.; Verdonschot, N.; Buma, P. Frictional and bone ingrowth properties of engineered surface topographies produced by electron beam technology. *Arch Orthop Trauma Surg* **2011**, 131, 711–718, DOI:10.1007/s00402-010-1218–1219.
9. O'Shea, K.; Quinlan, J.F.; Kutty, S.; Mulcahy, D.; Brady, O.H. The use of uncemented extensively porous-coated femoral components in the management of Vancouver B2 and B3 periprosthetic femoral fractures. *J Bone Joint Surg Br* **2005**, 87, 1617/*-621, DOI:10.1302/0301-620X.87B12.16338.
10. Giusti, A.; Hamdy, N.A.; Papapoulos, S.E. Atypical fractures of the femur and bisphosphonate therapy: A systematic review of case/case series studies. *Bone* **2010**, 47, 169–180, DOI:10.1016/j.bone.2010.05.019.
11. Koh, A.; Guerado, E.; Giannoudis, P.V. Atypical femoral fractures related to bisphosphonate treatment: issues and controversies related to their surgical management. *Bone Joint J* **2017**, 99-B, 295–302, DOI:10.1302/0301-620X.99B3.BJJ-2016-0276.R2.
12. Odvina, C.V.; Zerwekh, J.E.; Rao, D.S.; Maalouf, N.; Gottschalk, F.A.; Pak, C.Y. Severely suppressed bone turnover: a potential complication of alendronate therapy. *J Clin Endocrinol Metab* **2005**, 90, 1294–1301, DOI:10.1210/jc.2004-0952.
13. Nishino, T.; Hyodo, K.; Matsumoto, Y.; Yanagisawa, Y.; Yamazaki, M. Bisphosphonate-related atypical femoral fractures in patients with autoimmune disease treated with glucocorticoids: surgical results for 20 limbs. *J Clin Med* **2024**, 13, 1027, DOI:10.3390/jcm13041027.
14. Cho, J.W.; Oh, C.W.; Leung, F.; Park, K.C.; Wong, M.K.; Kwek, E.; Kim, H.J.; Oh, J.K. Healing of atypical subtrochanteric femur fractures after cephalomedullary nailing: which factors predict union. *J Orthop Trauma* **2017**, 31, 138–145, DOI:10.1097/BOT.0000000000000743.
15. Black, D.M.; Geiger, E.J.; Eastell, R.; Vittinghoff, E.; Li, B.H.; Ryan, D.S.; Dell, R.M.; Adams, A.L. Atypical femur fracture risk versus fragility fracture prevention with bisphosphonates. *N Engl J Med* **2020**, 383, 743–753, DOI:10.1056/NEJMoa1916525.
16. Byun, S.E.; Lee, K.J.; Shin, W.C.; Moon, N.H.; Kim, C.H. The effect of teriparatide on fracture healing after atypical femoral fracture: A systematic review and meta-analysis. *Osteoporos Int* **2023**, 34, 1323–1334, DOI:10.1007/s00198-023-06768-w.
17. Min, B.W.; Koo, K.H.; Park, Y.S.; Oh, C.W.; Lim, S.J.; Kim, J.W.; Lee, K.J.; Lee, Y.K. Scoring system for identifying impending complete fractures in incomplete atypical femoral fractures. *J Clin Endocrinol Metab* **2017**, 102, 545–550, DOI:10.1210/jc.2016-2787.

 doi:10.20944/preprints202409.0767.v1

18. Yee, D.; Cheng, H.C. Hip Arthroplasty for treatment of atypical femoral fracture with pre-existing hip osteoarthritis. Journal of Orthopaedics, Trauma and Rehabilitation. 2016, 21, 1–5. DOI:10.1016/j.jotr.2015.11.001.
19. Mondanelli, N.; Troiano, E.; Facchini, A.; Ghezzi, R.; Di Meglio, M.; Nuvoli, N.; Peri, G.; Aiuto, P.; Colasanti, G.B.; Giannotti, S. Treatment algorithm of periprosthetic femoral fracturens. *Geriatr Orthop Surg Rehabil* **2022**, 13, 21514593221097608, DOI:10.1177/21514593221097608.
20. Lewallen, D.G.; Berry, D.J. Periprosthetic fracture of the femur after total hip arthroplasty: treatment and results to date. *Instr Course Lect* **1998**, 47, 243–249.
21. Larson, J.E.; Chao, E.Y.; Fitzgerald, R.H. Bypassing femoral cortical defects with cemented intramedullary stems. *J Orthop Res* **1991**, 9, 414–421, DOI:10.1002/jor.1100090314.
22. Panjabi, M.M.; Trumble, T.; Hult, J.E.; Southwick, W.O. Effect of femoral stem length on stress raisers associated with revision hip arthroplasty. *J Orthop Res* **1985**, 3, 447–455, DOI:10.1002/jor.1100030407.